Geostationary satellite observations of dynamic phytoplankton photophysiology

Citation	O'Malley, R. T., Behrenfeld, M. J., Westberry, T. K., Milligan, A. J., Shang, S., & Yan, J. (2014). Geostationary satellite observations of dynamic phytoplankton photophysiology. Geophysical Research Letters, 41(14), 5052-5059. doi:10.1002/2014GL060246
DOI	10.1002/2014GL060246
Publisher	American Geophysical Union
Version	Version of Record
Terms of Use	http://cdss.library.oregonstate.edu/sa-termsofuse

AGU PUBLICATIONS

Geophysical Research Letters

RESEARCH LETTER
10.1002/2014GL060246

Key Points:
- Geostationary measurements reveal phytoplankton photoacclimation
- Cholorophyll fluorescence yields phytoplankton light saturation index (Ek)
- Phytoplankton photoacclimation is tuned to median mixed layer light level

Supporting Information:
- Readme
- Figures S1–S28
- Text S1

Correspondence to:
M. J. Behrenfeld,
mjb@science.oregonstate.edu

Citation:
O'Malley, R. T., M. J. Behrenfeld, T. K. Westberry, A. J. Milligan, S. Shang, and J. Yan (2014), Geostationary satellite observations of dynamic phytoplankton photophysiology, *Geophys. Res. Lett.*, *41*, 5052–5059, doi:10.1002/2014GL060246.

Received 16 APR 2014
Accepted 26 JUN 2014
Accepted article online 27 JUN 2014
Published online 17 JUL 2014

Geostationary satellite observations of dynamic phytoplankton photophysiology

Robert T. O'Malley[1], Michael J. Behrenfeld[1], Toby K. Westberry[1], Allen J. Milligan[1], Shaoling Shang[2], and Jing Yan[2]

[1]Department of Botany and Plant Pathology, Oregon State University, Corvallis, Oregon, USA, [2]State Key Laboratory of Marine Environmental Science, Xiamen University, Xiamen, China

Abstract Since June 2010, the Geostationary Ocean Color Imager (GOCI) has been collecting the first diurnally resolved satellite ocean measurements. Here GOCI retrievals of phytoplankton chlorophyll concentration and fluorescence are used to evaluate daily to seasonal changes in photophysiological properties. We focus on nonphotochemical quenching (NPQ) processes that protect phytoplankton from high light damage and cause strong diurnal cycles in fluorescence emission. This NPQ signal varies seasonally, with maxima in winter and minima in summer. Contrary to expectations from laboratory studies under constant light conditions, this pattern is highly consistent with an earlier conceptual model and recent field observations. The same seasonal cycle is registered in fluorescence data from the polar-orbiting Moderate Resolution Imaging Spectroradiometer Aqua satellite sensor. GOCI data reveal a strong correlation between mixed layer growth irradiance and fluorescence-derived phytoplankton photoacclimation state that can provide a path for mechanistically accounting for NPQ variability and, subsequently, retrieving information on iron stress in global phytoplankton populations.

1. Introduction

Every day, the ocean emits light of a biological origin: the fluorescence of chlorophyll *a* in phytoplankton. This signal has been globally monitored from space by the Moderate Resolution Imaging Spectrometer (MODIS) on NASA's Aqua satellite since July 2002. The distribution of solar-induced (i.e., natural) fluorescence reflects, to first order, patterns in surface chlorophyll concentration [*Behrenfeld et al*., 2009; *Letelier et al*., 1997]. However, physiological factors also have a strong impact on fluorescence variability. Pigment packaging effects [*Bricaud et al*., 1995], for example, cause chlorophyll-normalized fluorescence to decrease with increasing chlorophyll concentration [*Behrenfeld et al*., 2009]. Another critical process impacting MODIS fluorescence data is nonphotochemical quenching (NPQ). NPQ encompasses a variety of specific mechanism within photosynthetic membranes that thermally dissipate absorbed sunlight energy that is in excess of requirements for light-saturated photosynthesis [*Muller et al*., 2001]. Because MODIS ocean retrievals are only collected under clear-sky, high light conditions, observed fluorescence is strongly dampened by near-maximal NPQ levels [*Behrenfeld et al*., 2009; *Morrison and Goodwin*, 2010]. A third factor influencing fluorescence yields, which is of great ecological interest, is biologically available iron in the ocean surface layer. Iron stress in phytoplankton causes a significant increase in fluorescence emission, in part, owing to the associated synthesis of photosynthetically inactive chlorophyll pigment complexes [*Ryan-Keogh et al*., 2012; *Schrader et al*., 2011]. Resolving this latter physiological signature can allow global monitoring of surface ocean iron status, but achieving this goal first requires an accurate characterization of the NPQ effects.

In June 2010, the first Geostationary Ocean Color Imager (GOCI) was launched into space [*Ryu et al*., 2012]. GOCI provides daily retrievals of ocean properties in the northwestern Pacific at hourly resolution between 9:15 A.M. and 4:15 P.M. local time. These temporally resolved daily measurements offer an unprecedented opportunity to evaluate physiological variability in natural phytoplankton populations. The current study represents the first GOCI-based investigation of fluorescence variability. Our focus is on evaluating and constraining an earlier conceptual model of NPQ variability and its relation to photoacclimation states in phytoplankton [*Behrenfeld et al*., 2009]. While refinements are still needed in GOCI ocean radiance retrieval algorithms and data processing, our results strongly suggest that these unique observations will be highly valuable for further understanding the photophysiological properties of surface ocean phytoplankton populations.

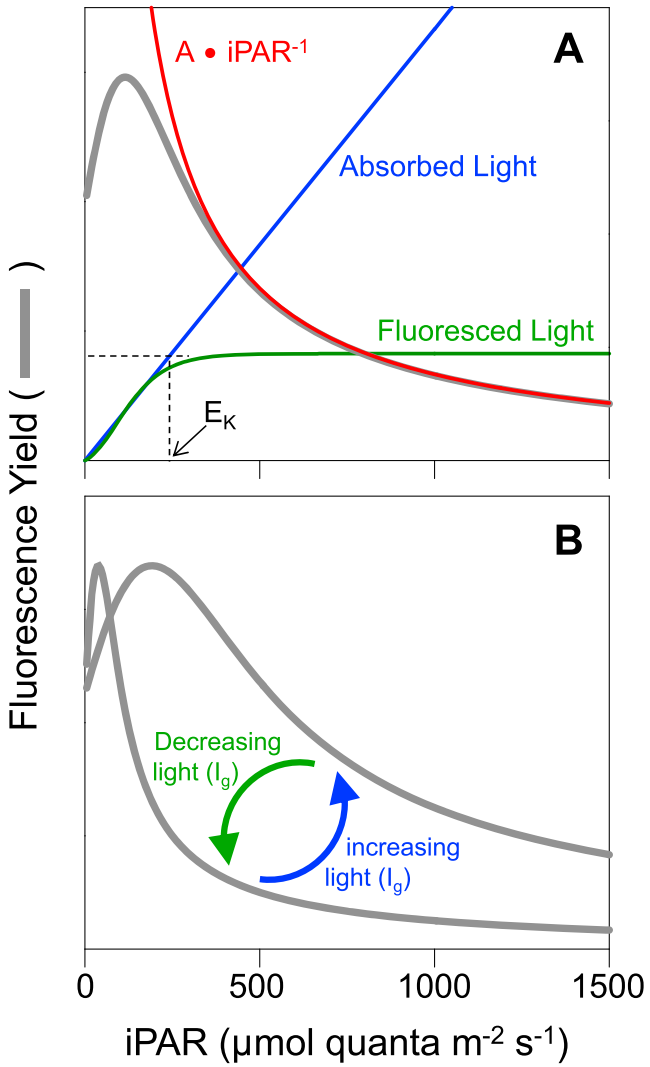

Figure 1. (a) Relationships between fluorescence yield and incident light (iPAR). Absorbed light is a linear function of incident light; fluoresced light is modeled as a hyperbolic tangent after *Jassby and Platt* [1976]. Fluorescence yield = fluoresced light/absorbed light. At high light levels, the fluorescence yield approximates a (1/iPAR) curve (red line = A · $iPAR^{-1}$). As the slope of the absorbed light changes, *Ek* shifts, and different values of A are needed to fit the resulting fluorescence yield curve. (b) Illustration of the changes in fluorescence yield due to photacclimation to different light regimes. Under low growth irradiance (*Ig*), the absorbed light curve steepens to bring in more light energy, *Ek* gets smaller, and NPQ processes are engaged sooner, resulting in a rapid (1/iPAR) dropoff in fluorescence yield. Under high *Ig* conditions the opposite takes place.

In photosynthetic organisms, the light energy absorbed by photosynthetic pigments increases linearly with increasing light intensity (blue line, Figure 1a). The energy absorbed by the oxygen-evolving photosystem II (PSII) complexes is the dominant source of satellite-detected natural fluorescence. Fluorescence yield (i.e., fluorescence emission per unit absorbed light energy) initially increases with light intensity as a progressively greater fraction of PSIIs become photochemically oxidized (gray line, Figure 1a). When photosynthesis approaches light saturation, NPQ mechanisms are engaged that intercept energy transfer between light-harvesting antennae pigments and PSII core pigments. As described in *Behrenfeld et al.* [2009], a perfect match between excess light energy absorption and thermal dissipation will result in a constant high-light fluorescence emission (green line, Figure 1a) and an NPQ-driven reduction in fluorescence yield that follows an inverse function of the incident photosynthetically active radiation (iPAR) level (red line, Figure 1a). An NPQ response that exceeds this $iPAR^{-1}$ relationship (i.e., $iPAR^{-n}$, where $n > 1$) is unexpected, as it would imply light-limited photosynthesis at high iPAR. However, an NPQ response weaker than $iPAR^{-1}$ (i.e., $iPAR^{-n}$, where $n < 1$) has been observed in the field and laboratory [*Laney et al.*, 2005; *Letelier et al.*, 1997; *Milligan et al.*, 2012; *Morrison*, 2003; *Schallenberg et al.*, 2008], which consequently yields a modest but steady rise in fluorescence emission with increasing light. GOCI data provide an opportunity to constrain this range in NPQ response slopes for natural phytoplankton assemblages.

In *Behrenfeld et al.* [2009], global patterns of phytoplankton iron stress were evaluated using MODIS fluorescence data, where a single $iPAR^{-1}$ function was used to correct for NPQ effects. A recommendation from this study was that future revisions to the NPQ correction focus, in particular, on photoacclimation effects. In the laboratory, NPQ is greater in phytoplankton photoacclimated to constant high light compared to low light [*Garcia-Mendoza et al.*, 2002; *García-Mendoza and Colombo-Pallotta*, 2007; *Niyogi et al.*, 1997; *Ragni et al.*, 2008]. Nevertheless, *Behrenfeld et al.* [2009] proposed an opposite relationship for natural populations. Specifically, they hypothesized that phytoplankton in a deep mixed layer will have elevated chlorophyll concentrations relative to a shallow mixed layer but consequently will also require enhanced NPQ protection against high light exposure near the surface (Figure 1b). *Morrison and Goodwin* [2010] subsequently

evaluated seasonal variability in MODIS fluorescence data for the Gulf of Maine and reported a significant effect of photoacclimation on fluorescence yields consistent with *Behrenfeld et al.* [2009]. *Milligan et al.* [2012] grew laboratory phytoplankton cultures under simulated mixing conditions and also found greater NPQ capacities for their deeper-mixing scenario. More recently, *Browning et al.* [2014] observed increasing NPQ with decreasing mixed layer light levels in Southern Ocean phytoplankton assemblages. In the current analysis, we verify the presence of a generalized NPQ correction in the daily fluorescence efficiencies (F^* = fluorescence chlorophyll^{-1}) and compare seasonal changes in GOCI-observed fluorescence efficiencies to changes in mixed layer growth irradiances (I_g = median daily mixed layer photosynthetically active radiation (PAR)) to further evaluate the photoacclimation effect on NPQ.

2. Data and Methodology

2.1. GOCI Satellite Data

GOCI has eight measurement channels centered at 412, 443, 490, 555, 660, 680, 745, and 865 nm, with each having a 20 nm bandwidth except the fluorescence channel (680 nm) which has a 10 nm bandwidth to avoid overlap with the 660 nm band and an atmospheric O_2 absorption feature centered at 687 nm. Standard Level-2 GOCI-derived ocean products provided by the Korea Ocean Satellite Center (KOSC) include normalized water leaving radiances (nL_W) for each channel and chlorophyll concentration (Chl). Fluorescence line height (FLH) values were calculated as the difference between measured nL_W at 680 nm and a baseline value for 680 nm determined by linear extrapolation of nL_W measured for the 660 and 745 nm bands [*Abbott and Letelier*, 1999].

GOCI data are collected using a 2-D staring-frame capture method [*Ryu et al.*, 2012]. With this approach, the observing area is divided into 16 acquisition and processing bins, or "slots" (numbered 0 to 15), each with ~500 m pixel resolution (Figure 2a). The current analysis was restricted to data for open ocean slots 12 and 13 to avoid the potential compromising effects of suspended sediments on fluorescence retrievals closer to land [*Gower et al.*, 1999]. Data within slots 12 and 13 were subsampled (large boxes in Figure 2b) to avoid the apparent FLH retrieval artifacts in the southernmost pixels of each slot (e.g., red pixels in Figure 2b) [*Oh et al.*, 2012]. Within the subsample region, any pixel with an FLH value > 1 (W m^{-2} μm^{-1} sr^{-1}) was flagged as unreliable.

The intent of the current study was to conduct an initial investigation of fluorescence variability using geostationary satellite data, not an extensive evaluation of the GOCI ocean color record. Accordingly, we limited our analysis to specific dates with minimum cloud cover over the full day. For bin 13, this selection provided daily cycles in Chl and FLH for winter (20 December 2012), spring (6 May 2012), summer (19 June 2011), and autumn (27 September 2011). For bin 12, persistent cloudiness limited our analysis to 5 August 2011, 27 September 2011, 26 November 2012, and 20 December 2012.

2.2. Supporting Data

In addition to FLH and Chl observations, evaluation of NPQ variability requires temporally resolved iPAR data and estimates of mixed layer I_g. iPAR and PAR are standard products for MODIS Aqua but are not currently produced from GOCI data. MODIS iPAR data (μmoles quanta m^{-2} s^{-1}) were therefore projected onto the GOCI grid and values for each GOCI observational time point calculated by fitting a sunrise-to-sunset half-sine curve through the MODIS iPAR values (~13:36 h). Inaccuracies in this approach are small for clear-sky scenes (i.e., when ocean color retrievals are made) relative to daily and seasonal changes in incident light. MODIS daily PAR data (moles quanta m^{-2} d^{-1}) were also used to calculate I_g (moles quanta m^{-2} h^{-1}) following *Behrenfeld et al.* [2005] (see supporting information).

GOCI-derived fluorescence properties were also compared to MODIS Aqua retrievals. For this comparison, daily Level-3 MODIS fluorescence products (9 km resolution) were obtained from the NASA Ocean Color website (http://oceancolor.gsfc.nasa.gov/) and averaged over the GOCI analysis bins (black boxes in Figure 2b). The intent of this analysis was to evaluate consistencies in seasonal patterns between the two sensors. A priori, quantitative differences are expected between MODIS and GOCI fluorescence products. First, the GOCI fluorescence band (680 nm center) is better aligned with the PSII fluorescence emission peak at 685 nm than the MODIS fluorescence band (678 nm center). However, the GOCI band is also impacted more by the atmospheric oxygen absorption feature. In addition, the MODIS sensor has been operational for over a decade, which has allowed far more time for sensor characterization and data reprocessing than for the 2 year old GOCI sensor.

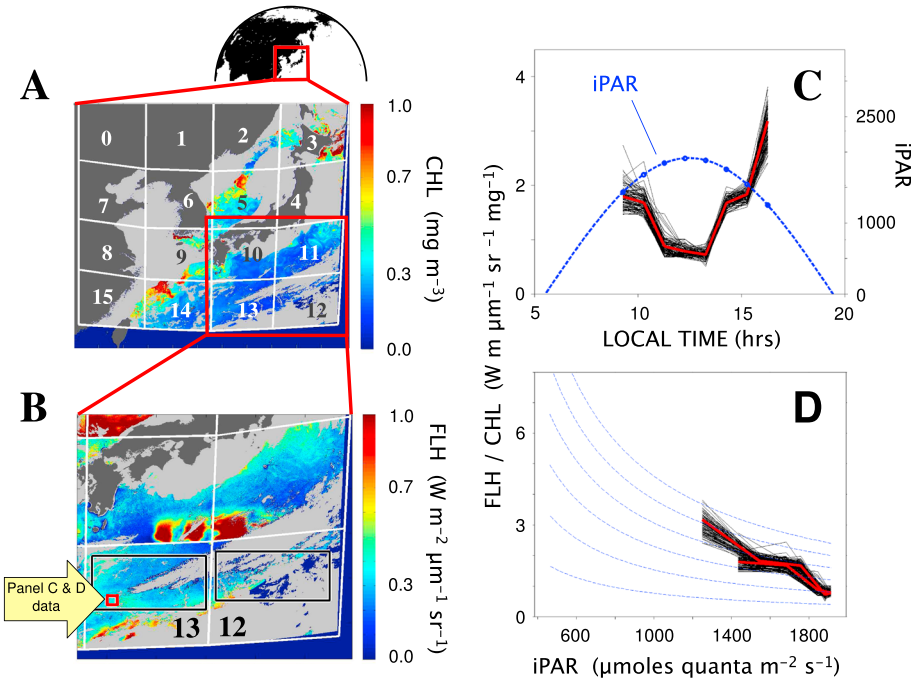

Figure 2. (a) Chlorophyll map (6 May 2012, 09:15 local time): dark gray land masses; light gray cloud coverage. We show a representation of acquisition and processing slots 0–15. See Figure 3b from *Ahn et al.* [2012] for the specific geometry. (b) Fluorescence line height (FLH) coverage for slots 12 and 13, same time period as Figure 2a. FLH is a residual calculation sensitive to the radiance discrepancies between slots, as seen by the red areas above slot 13. Boundaries for data analysis (black boxes) were chosen to avoid such regions. The small red box shows the data location for Figures 2c and 2d. (c) FLH/CHL data extracted from the $(50\ \text{km})^2$ area box shown in Figure 2b. The thick red line indicates the average for the area; fine black lines give averages for the $(5\ \text{km})^2$ subgrids comprising the area. A half-sine curve through sunrise and sunset is scaled to overlay MODIS iPAR. The effect of NPQ processes is clearly visible in the inverse relationship between iPAR and FLH/CHL. (d) The FLH/CHL data in Figure 2c replotted with respect to iPAR. Afternoon values are fluorescing at levels greater than their morning counterparts at the same level of light, indicating an effect of hysteresis following extreme midday light exposure. Various $\{A \cdot \text{iPAR}^{-1}\}$ curves are drawn to span the data.

2.3. Assessment of Photoacclimation State

For a phytoplankton acclimated to a given I_g and exposed to increasing iPAR, photosynthetic electron transport initially increases linearly at subsaturating light levels in proportion to the product of iPAR and the maximum PSII photon-capturing efficiency, α_{PC}. At saturating light levels, photosynthetic electron transport reaches a maximum rate, P_{max}, that is largely defined by the capacity of the Calvin cycle reactions [*Stitt*, 1986]. Phytoplankton respond to a change in I_g by adjusting the balance between α_{PC} and P_{max}. For example, a decrease in I_g results in an increase in α_{PC} and a consequent decrease in the light intensity necessary to saturate photosynthesis. This photoacclimation response is commonly quantified as a change in the saturation index, $E_k = P_{max}/\alpha_{PC}$. Variability in E_k has a direct impact on the relationship between fluorescence emission and iPAR.

Fluorescence yield (F.Y.) is the ratio of fluorescence emission (F) to absorbed light, where F is defined by the rate of photon energy transfer to PSII and the probability of energy loss to fluorescence (f_{eff}). Thus, $F = f_{eff} \cdot P_{max}$ at saturating iPAR. The rate of light absorption, on the other hand, is defined by the product, $\alpha_{PC} \cdot \text{iPAR}$. At light saturation, therefore,

$$\text{F.Y.} = (f_{eff} \cdot P_{max})/(\alpha_{PC} \cdot \text{iPAR}) = f_{eff} \cdot (P_{max}/\alpha_{PC}) \cdot \text{iPAR}^{-1} = f_{eff} \cdot E_k \cdot \text{iPAR}^{-1}. \quad (1)$$

Rearranging (1) gives

$$E_k = (\text{F.Y.} \cdot \text{iPAR})/f_{eff}. \quad (2)$$

Thus, GOCI-observed variability in fluorescence yields as a function of iPAR can be equated to photoacclimation-driven changes in E_k, which subsequently can be evaluated in terms of variability in I_g. For

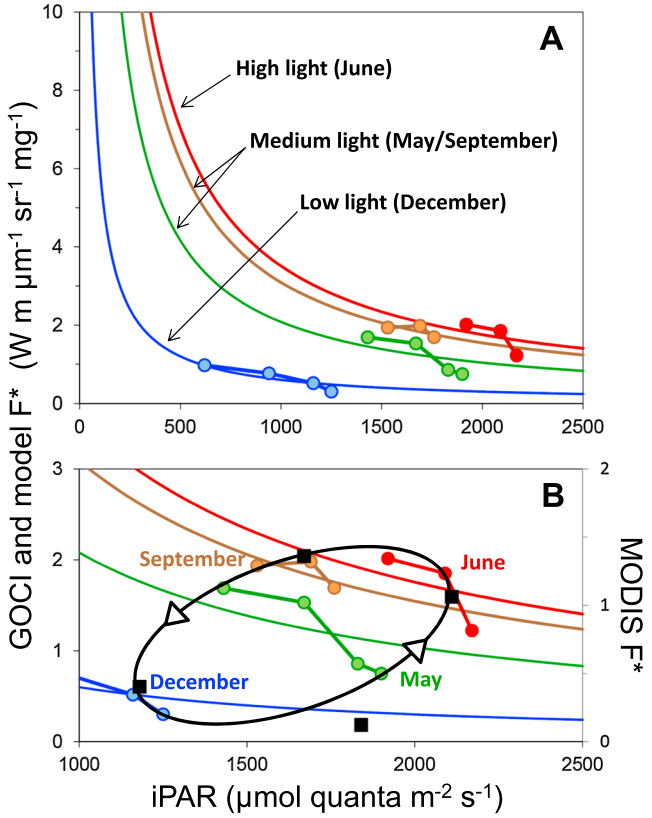

Figure 3. (a) Results for the 300 km × 575 km averaging area in slot 13 (black box, Figure 2b). $F^* = \mathrm{FLH/CHL}$. Model curves shown represent RMS best fits of $\{A \cdot \mathrm{iPAR}^{-1}\}$ curves to the hourly data points. The transition from low light (December) to high light (June) is clearly visible. (b) MODIS values (black squares) along with GOCI results of Figure 3a. MODIS values have been scaled to overlay the GOCI results. The black ellipse shows the annual orbit traced out by the fluorescence yield in the transition from low light to high light and back again and is seen in both data sets.

this analysis, we assumed a value for f_{eff} of 1.4%, which represents the global median from *Behrenfeld et al.* [2009] (see their Figures 5a and 5d). It should be noted that E_k values derived from this approach are based on fluorescence. E_k based on fluorescence will always be less than or equal to E_k of carbon fixation [*Laney et al.*, 2005; *Milligan et al.*, 2012]. Finally, we also used GOCI data to evaluate potential constraints on the power of the NPQ response function for natural phytoplankton populations (i.e., iPAR^{-n}). Specifically, observed seasonal changes in fluorescence efficiencies were fit using NPQ response powers ranging from −1 to −0.5 and then associated ranges in E_k calculated from (2) were evaluated in terms of measured E_k variability in the field.

3. Results and Discussion

Nonphotochemical quenching is a rapidly reversible protective response in photosynthetic organisms to supersaturating light levels that results in a dampening of fluorescence emission. Accordingly, it has long been recognized that NPQ causes an inverse relationship between fluorescence and iPAR [*Kautsky and Hirsch*, 1931; *Kiefer*, 1973; *Laney et al.*, 2005]. However, fluorescence emission also varies with chlorophyll concentration. Accordingly, normalizing fluorescence to chlorophyll (F^*) better isolates the NPQ effect from this dependence on changing pigment concentration. An example GOCI-observed diurnal cycle in F^* is shown in Figure 2c. This particular time course corresponds to a nearly cloud-free 50 km × 50 km area in processing slot 13 on 6 May 2012 (small outlined red box in Figure 2b). These data clearly show the anticipated inverse relationship between F^* and iPAR, thus representing the first characterization of diurnal NPQ variability from space. While the midday suppression of F^* is far from a novel finding, the advantage provided by GOCI is an ability to continuously monitor such NPQ changes over broad regions and throughout the year.

The decrease in fluorescence from dawn to midday and its recovery in the afternoon (Figure 2c) is not only simply dependent on iPAR but is also influenced by time scales of induction and relaxation for specific NPQ mechanisms and changing cellular demands for photosynthetic products. These factors cause the relaxation of NPQ from noon to sunset to follow a slightly offset pattern with respect to iPAR compared to the NPQ induction phase from sunrise to noon (Figure 2c). In other words, changes in cellular processes over the diurnal cycle give rise to a temporal hysteresis in the daily iPAR- F^* relationship. This hysteresis has been previously observed in the laboratory and field [*Laney et al.*, 2005; *Levy et al.*, 2004; *Neale*, 1987] and is also apparent in the GOCI F^* data. For example, while the time course shown in Figure 2c is relatively symmetric around noon, replotting these F^* data as a function of iPAR reveals a modest hysteresis, with fluorescence slightly elevated in the afternoon for a given iPAR value (Figure 2d). In general, we found this hysteresis to be stronger during summer months and weaker in winter.

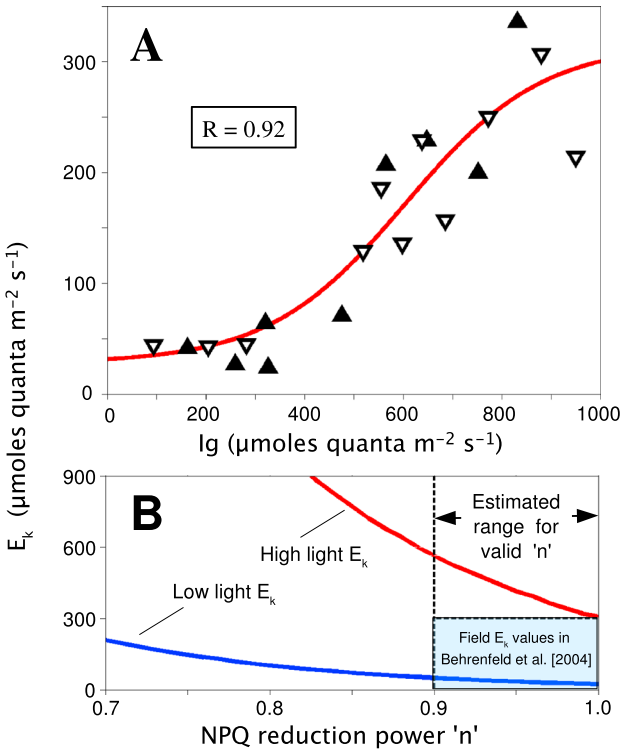

Figure 4. (a) Summary plot of *Ig* versus *Ek*, based on best fit curves for slots 12 and 13 using specific *Ig* zones (see supporting information). Open triangles show data from slot 13; closed triangles show data from slot 12 (see Figure 2b for location of data selection areas). A hyperbolic tangent was fit to the data. (b) A high light and low light examples are solved for *Ek* based on best fit $\{A \cdot iPAR^{-n}\}$ curves for different values of "*n*." A conservative estimate suggests that the factor is somewhere between 0.9 and 1.0 for this region.

For our analysis of seasonal photoacclimation effects, we removed the impact of hysteresis in daily F^* variability by focusing on data during the morning-to-midday NPQ induction period. GOCI processing slot 13 provided a reasonably cloud-free daily time course in F^* for each season (see above). For these 4 days, we compared F^* time series for data averaged over a 300 km × 575 km area (large outlined black box in slot 13 of Figure 2b). For each time point in this analysis, only pixels with FLH, Chl, and iPAR data were included in the bin average, and bin values were only calculated if more than 100 such pixels were available for averaging. Despite the relatively large bin size, these criteria prevented valid retrievals for the 9:15 time point on 19 June and 27 September (i.e., too cloudy).

If the physiological status of phytoplankton were held constant throughout the year, then F^* would be maximal in winter and minimal in summer simply due to the higher iPAR in summer driving stronger NPQ. In contrast to this scenario, GOCI results show a clear seasonal pattern of increasing F^* from winter to summer and decreasing F^* from summer to winter (Figures 3a and 3b). Indeed, June F^* values were a factor of ~2 greater than December values, despite iPAR being twice as high in June. This finding implies that seasonal photoacclimation has a significant impact on the NPQ response. Specifically, phytoplankton in the GOCI observational region experience deeper mixing and lower daily PAR in December compared to June. Accordingly, the December population is photoacclimated to lower values of I_g, becomes light saturated at lower iPAR, and thus requires greater NPQ protection when exposed to surface light intensities (which by midday exceed 1000 µmoles quanta m^{-2} s^{-1}) (Figures 1b and 3a). This photoacclimation response is further illustrated by fitting (i.e., minimizing root-mean-square (RMS) error) an $iPAR^{-1}$ curve to the seasonal GOCI data (Figure 3a). The resultant relationships show a seasonal pattern consistent with the conceptual model of *Behrenfeld et al.* [2009] (Figure 1b).

GOCI geostationary observations allow a far more detailed evaluation of daily NPQ dynamics than a polar-orbiting ocean color sensor (approximately one observation per day at midlatitudes), but both types of sensors will register photoacclimation-driven changes in F^* over the annual cycle [*Morrison and Goodwin*, 2010]. Comparison of our seasonal GOCI data with corresponding F^* values from MODIS Aqua (Figure 3b) illustrates the expected (see above) quantitative difference in F^* values for the two sensors (i.e., right axis versus left axis). More importantly, this comparison illustrates a highly consistent seasonal cycle in photoacclimation-driven changes in fluorescence yields (black line, Figure 3b).

As described above, the suppression of F^* with decreasing I_g is consistent with lower light saturation of photosynthetic electron transport and, accordingly, earlier induction of NPQ. This relationship can be quantified by comparing mixed layer I_g values with changes in the light-saturation index, E_k. For this comparison, we used data from both analysis bins (large boxes in Figure 2b) in slots 12 and 13 and, within each slot and for each daily time course, separated data into categories of low, medium, and high I_g (see supporting information). For

each date and I_g category, E_k was calculated from GOCI F^* data using (2). Assuming an NPQ response following an iPAR^{-1} function, we retrieve E_k values ranging from ~25 to ~300 μmoles quanta m^{-2} s^{-1} and find that the variability in E_k is highly correlated with I_g ($r = 0.92$; Figure 4a). Our I_g-E_k relationship suggests a dampened sensitivity of E_k at very low and very high values of I_g and a strong, essentially linear response over a range of moderate I_g values (Figure 4a). We also repeated these calculations using NPQ response powers ranging from −0.95 to −0.5 (i.e., iPAR^{-n}, where $n < 1$), which effectively represents a decreasing efficiency in the quenching of excess excitation energy between light-harvesting antennae and PSII core antennae (see above). Modifying the NPQ response power from −1 to −0.5 does not weaken the retrieved relationship between I_g and E_k, but it does significantly change the range of calculated E_k values (Figure 4b). This analysis can thus provide some constraint on the potential range of valid NPQ slope values because E_k variability has been extensively measured in the field using ^{14}C-based photosynthesis-irradiance (PI) measurements. For example, *Behrenfeld et al*. [2004] compiled over 1200 global PI measurements collected under conditions ranging from very low light, low-temperature Southern Ocean stations to high-light, high-temperature conditions in the South Pacific gyre. For their data set, 99% of the measured E_k values were < 300 μmoles quanta m^{-2} s^{-1}. Comparing this value to the E_k ranges shown in Figure 4b suggests that very conservatively, the potentially valid range of NPQ response powers for the GOCI data is around −0.9 to −1. Additional field and satellite analyses are needed to further evaluate this constraint over a broader ocean area.

4. Conclusions

The current study represents an initial investigation on daily to seasonal dynamics in phytoplankton photophysiology using geostationary satellite data. Our results, first and foremost, highlight the potential of GOCI's unique, time-resolved ocean color measurements, a potential that will only improve with future advances in GOCI data processing. In recognition of this potential, the KOSC has recently teamed with the NASA Goddard Space Flight Center's Ocean Color Group to accelerate data processing developments. Our results also demonstrate the significant impacts of photoacclimation on fluorescence variability and are consistent with the conceptual model of *Behrenfeld et al*. [2009] and results of *Morrison and Goodwin* [2010] for the Gulf of Maine. We find that acclimation to decreased mixed layer light levels is associated with an increased capacity for near-surface nonphotochemical quenching and that the power of the iPAR-NPQ response is roughly constrained between −0.9 and −1.0. In addition to gaining insights on phytoplankton photoprotection, the accurate characterization of NPQ is also critical for removing this source of variability from satellite-retrieved fluorescence data and recovering additional physiological information, such as iron stress. To this end, the similarity in seasonal F^* variability between GOCI and MODIS Aqua data suggests that further analysis of the latter data set may allow for a truly global assessment of F^* variability as a function of photoacclimation state.

Acknowledgments
GOCI data was provided by the Korea Ocean Satellite Center (KOSC)/KORDI. This study was supported by the National Aeronautics and Space Administration Ocean Biology and Geochemistry Program.

The Editor thanks two anonymous reviewers for their assistance in evaluating this paper.

References

Abbott, M. R., and R. M. Letelier (1999), Algorithm theoretical basis document chlorophyll fluorescence (MODIS product number 20), *Rep*., NASA.

Ahn, J. H., Y. J. Park, J. H. Ryu, B. Lee, and I. S. Oh (2012), Development of Atmospheric Correction Algorithm for Geostationary Ocean Color Imager (GOCI), *Ocean Sci. J*., *47*(3), 247–259.

Behrenfeld, M. J., O. Prasil, M. Babin, and F. Bruyant (2004), In search of a physiological basis for covariations in light-limited and light-saturated photosynthesis, *J. Phycol*., *40*(1), 4–25.

Behrenfeld, M. J., E. Boss, D. A. Siegel, and D. M. Shea (2005), Carbon-based ocean productivity and phytoplankton physiology from space, *Global Biogeochem. Cycles*, *19*, GB1006, doi:10.1029/2004GB002299.

Behrenfeld, M. J., et al. (2009), Satellite-detected fluorescence reveals global physiology of ocean phytoplankton, *Biogeosciences*, *6*(5), 779–794.

Bricaud, A., M. Babin, A. Morel, and H. Claustre (1995), Variability in the chlorophyll-specific absorption-coefficients of natural phytoplankton: Analysis and parameterization, *J. Geophys. Res*., *100*(C7), 13,321–13,332, doi:10.1029/95JC00463.

Browning, T. J., H. A. Bouman, and C. M. Moore (2014), Satellite-detected fluorescence: Decoupling non-photochemical quenching from iron stress signals in the South Atlantic and Southern Ocean, *Global Biogeochem. Cycles*, *28*, 510–524, doi:10.1002/2013GB004773.

García-Mendoza, E., and M. F. Colombo-Pallotta (2007), The giant kelp *Macrocystis pyrifera* presents a different nonphotochemical quenching control than higher plants, *New Phytol*., *173*(3), 526–536.

Garcia-Mendoza, E., H. Matthijs, H. Schubert, and L. Mur (2002), Non-photochemical quenching of chlorophyll fluorescence in *Chlorella fusca* acclimated to constant and dynamic light conditions, *Photosynth. Res*., *74*(3), 303–315.

Gower, J. F. R., R. Doerffer, H. Schubert, and G. A. Borstad (1999), Interpretation of 685 nm peak in water-leaving radiance spectra in terms of fluorescence, absorption and scattering, and its observation by MERIS, *Int. J. Remote Sens*., *20*(9), 1771–1786.

Jassby, A. D., and T. Platt (1976), Mathematical formulation of the relationship between photosynthesis and light for phytoplankton, *Limnol. Oceanogr*., *21*, 540–547.

Kautsky, H., and A. Hirsch (1931), Neue Versuche zur Kohlensäureassimilation, *Naturwissenschaften*, *19*, 964–964.

Kiefer, D. A. (1973), Fluorescence properties of natural phytoplankton populations, *Mar. Biol.*, *22*(3), 263–269.
Laney, S. R., R. M. Letelier, and M. R. Abbott (2005), Parameterizing the natural fluorescence kinetics of *Thalassiosira weissflogii*, *Limnol. Oceanogr.*, *50*(5), 1499–1510.
Letelier, R. M., M. R. Abbott, and D. M. Karl (1997), Chlorophyll natural fluorescence response to upwelling events in the Southern Ocean, *Geophys. Res. Lett.*, *24*(4), 409–412, doi:10.1029/97GL00205.
Levy, O., Z. Dubinsky, K. Schneider, Y. Achituv, D. Zakai, and M. Y. Gorbunov (2004), Diurnal hysteresis in coral photosynthesis, *Mar. Ecol. Prog. Ser.*, *268*, 105–117.
Milligan, A. J., U. A. Aparicio, and M. J. Behrenfeld (2012), Fluorescence and nonphotochemical quenching responses to simulated vertical mixing in the marine diatom *Thalassiosira weissflogii*, *Mar. Ecol. Prog. Ser.*, *448*, 67–78.
Morrison, J. R. (2003), In situ determination of the quantum yield of phytoplankton chlorophyll *a* fluorescence: A simple algorithm, observations, and a model, *Limnol. Oceanogr.*, *48*(2), 618–631.
Morrison, J. R., and D. S. Goodwin (2010), Phytoplankton photocompensation from space-based fluorescence measurements, *Geophys. Res. Lett.*, *37*, L06603, doi:10.1029/2009GL041799.
Muller, P., X. P. Li, and K. K. Niyogi (2001), Non-photochemical quenching. A response to excess light energy, *Plant Physiol.*, *125*(4), 1558–1566.
Neale, P. J. (1987), Algal photoinhibition and photosynthesis in the aquatic environment, in *Photoinhibition*, edited by D. J. Kyle, C. B. Osmond, and C. J. Arntzen, pp. 39–65, Elsevier, Amsterdam, Netherlands.
Niyogi, K. K., O. Bjorkman, and A. R. Grossman (1997), *Chlamydomonas* xanthophyll cycle mutants identified by video imaging of chlorophyll fluorescence quenching, *Plant Cell*, *9*(8), 1369–1380.
Oh, E., J. Hong, S.-W. Kim, S. Cho, and J. H. Ryu (2012), Stray light analysis of nearby slot source using integrated ray tracing technique, paper presented at Proc. SPIE 8533, Sensors, Systems, and Next-Generation Satellites XVI, doi:10.1117/12.974455.
Ragni, M., R. L. Airs, N. Leonardos, and R. J. Geider (2008), Photoinhibition of PSII in *Emiliania huxleyi* (Haptophyta) under high light stress: The roles of photoacclimation, photoprotection, and photorepair, *J. Phycol.*, *44*(3), 670–683.
Ryan-Keogh, T. J., A. I. Macey, A. M. Cockshutt, C. M. Moore, and T. S. Bibby (2012), The cyanobacterial chlorophyll-binding-protein ISIa acts to increase the in vivo effective absorption cross-section of PSI under iron limitation, *J. Phycol.*, *48*(1), 145–154.
Ryu, J. H., H. J. Han, S. Cho, Y. J. Park, and Y. H. Ahn (2012), Overview of geostationary ocean color imager (GOCI) and GOCI data processing system (GDPS), *Ocean Sci. J.*, *47*(3), 223–233.
Schallenberg, C., M. R. Lewis, D. E. Kelley, and J. J. Cullen (2008), Inferred influence of nutrient availability on the relationship between sun-induced chlorophyll fluorescence and incident irradiance in the Bering Sea, *J. Geophys. Res.*, *113*, C07046, doi:10.1029/2007JC004355.
Schrader, P. S., A. J. Milligan, and M. J. Behrenfeld (2011), Surplus photosynthetic antennae complexes underlie diagnostics of iron limitation in a cyanobacterium, *PLoS One*, *6*(4), doi:10.1371/journal.pone.0018753.
Stitt, M. (1986), Limitation of photosynthesis by carbon metabolism 1. Evidence for excess electron-transport capacity in leaves carrying out photosynthesis in saturating light and CO_2, *Plant Physiol.*, *81*, 1115–1122.